Transportation Research Part D 60 (2018) 41–55

Contents lists available at ScienceDirect

Transportation Research Part D

journal homepage: www.elsevier.com/locate/trd

Macroscopic modeling approach to estimate traffic-related emissions in urban areas

Yan-Qun Jiang [a,b,*], Pei-Jie Ma [a], Shu-Guang Zhou [c]

[a] School of Science, Southwest University of Science and Technology, Mianyang, Sichuan, China
[b] Key Laboratory for Thermal Science and Power Engineering of Ministry of Education, Department of Engineering Mechanics, Tsinghua University, Beijing, China
[c] China Aerodynamics Research and Development Center, Mianyang, Sichuan, China

ARTICLE INFO

Article history:
Received 4 August 2015
Revised 24 September 2015
Accepted 29 October 2015
Available online 2 December 2015

Keywords:
Macroscopic DTA model
Instantaneous emission model
Urban traffic flow
Traffic-related emissions
Discontinuous Galerkin method

ABSTRACT

This paper integrates a macroscopic dynamic traffic assignment (DTA) model for urban traffic flow with an instantaneous emission model to investigate traffic-related emissions in urban areas of arbitrary shape. It is assumed that homogeneous travelers continuously distributed over the urban areas tend to choose a path to minimize their total travel cost based on instantaneous traffic information. The macroscopic DTA model consists of a two-dimensional hyperbolic system of nonlinear conservation laws with source terms and an Eikonal-type equation used to describe the path-choice behavior of travelers. A solution algorithm for the model is designed as a Runge–Kutta Discontinuous Galerkin method for the hyperbolic system coupled with a fast sweeping method for the Eikonal-type equation on unstructured meshes. A case study investigating macroscopic characteristics of urban traffic flow and predicting exhaust emissions emitted by various types of vehicles in urban areas is conducted to illustrate the applicability of the model and the effectiveness of the algorithm.

Introduction

The contribution of road traffic in urban areas to current global anthropogenic emissions, such as carbon dioxide (CO_2), nitrogen oxides (NO_x), volatile organic compounds (VOC) and particulate matter (PM), is significant (Niemeier et al., 2006). These traffic-induced emissions have enormous impacts on human health and climate change. Therefore, previous research (Ahn et al., 2002; Panis et al., 2006; Smit et al., 2007; Nejadkoorki et al., 2008; Misra et al., 2013; Jie et al., 2013; Yin et al., 2012; Zegeye et al., 2013; Zhu, 2013; Tang et al., 2015; Yu and Shi, 2015) has focused on the contribution of traffic-generated air pollutants (e.g., NO_x, VOC and PM) and greenhouse gases (e.g., CO_2). Various modeling approaches of emission from motor vehicle exhausts including analytical models, numerical models and statistical models (Sharma and Khare, 2001; Smit et al., 2010) have been proposed over the years to evaluate the environmental effectiveness of various traffic management and traffic control strategies.

Most methodologies of calculating traffic-related emissions are based on emissions factors representing emissions emitted by each vehicle category under normal traffic conditions and operational parameters (e.g., the density, average speed and acceleration of traffic flows) representing real-world traffic conditions (Cortés et al., 2008). The literature encompasses two general approaches used to estimate vehicle emissions and fuel consumption (as represented by the CO_2 emissions): the

* Corresponding author at: School of Science, Southwest University of Science and Technology, Mianyang, Sichuan, China.
E-mail addresses: jyq2005@mail.ustc.edu.cn, yqjiang2014@126.com (Y.-Q. Jiang), peijie@mail.ustc.edu.cn (P.-J. Ma), zhousgcfd@sina.com (S.-G. Zhou).

http://dx.doi.org/10.1016/j.trd.2015.10.022
1361-9209/

macroscopic modeling approach and the microscopic modeling approach (Nejadkoorki et al., 2008). The macroscopic modeling approach uses average aggregate network parameters to estimate network-wide emission rates according to high-level relationships among density, flow, and speed of traffic flows on urban road networks (Dia et al., 2006). This approach is low-accuracy, but allows to compute faster the estimates of emissions. Therefore, macroscopic emission models, such as U.S. federal's MOBILE model (EPA, 2003), California's EMFAC model (CARB, 2007) and European's COPERT III model (Ntziachristos and Samaras, 2000), are useful for estimating the emissions of large-scale areas. However, these models ignore microscopic vehicle movement and could incorrectly estimate emission rates (Misra et al., 2013). The microscopic modeling approach is usually adopted to estimate instantaneous vehicle emission rates using either vehicle engine or vehicle speed/acceleration data. Microscopic emission models, such as the CMEM model (Barth et al., 2000), the VT-Micro model (Ahn et al., 2002), the VERSIT + model (Smit et al., 2007) and the MOVES model (Vallamsundar and Lin, 2011), are considered to be preferable for predicting emissions in urban areas. This is because the density and speed of traffic flows on networks can vary significantly over relatively short distance and time scales (Nejadkoorki et al., 2008).

Vehicle operational parameters that affect greatly the exhaust emissions are generally obtained by traffic surveys and dynamic traffic assignment (DTA) models. The former can most accurately reflect real-time traffic conditions, but is usually carried out on some specific road links and during a specific time period (Xia and Shao, 2005). Therefore, traffic surveys are often insufficient for adequately quantifying the traffic on the whole road network. DTA models that deal with time-varying flows can capture traffic dynamics on urban road networks (e.g., time-dependent travel speeds of vehicles), which is important input data required for the calculation of traffic emissions. There are two basic types of DTA models in literature, i.e., microscopic DTA models and macroscopic DTA models (Jiang et al., 2011). Microscopic DTA models as described in the review articles by Peeta and Ziliaskopoulos (2001), Szeto and Wong (2012), in which each individual vehicle is represented and each road link is modeled separately, are commonly adopted for the detailed planing and analysis of a transportation system. There are obviously difficulties in modeling a large-scale congested urban traffic network with a large number of links. Conversely, macroscopic DTA models (Rossa et al., 2010; Jiang et al., 2011; Tao et al., 2014; Saumtally et al., 2013), in which a dense network is approximated as a continuum on which travelers are free to choose their paths in a two-dimensional (2D) continuous space, are used in regional studies and for modeling highly dense transportation systems. Most of macroscopic DTA models (Rossa et al., 2010; Jiang et al., 2011; Tao et al., 2014) are derived from the classical Lighthill–Whitham–Richards (LWR) models for one-dimensional (1D) vehicular traffic flow and cannot express the acceleration/deceleration dynamics of vehicles. There are also developments combining ideas from both macroscopic and microscopic DTA models (Osorio and Nanduri, 2015).

In consideration of their capability of capturing the effect of traffic variations, DTA models integrated with road traffic emission models can characterize the traffic fluxes and quantify the emission amounts on an urban road network. Consequently, this type of integrated models, which typically consist of a microscopic/macroscopic DTA model and a microscopic/-macroscopic emission model (Xia and Shao, 2005; Panis et al., 2006; Pataki et al., 2009; Madireddy et al., 2011; Misra et al., 2013; Jie et al., 2013; Yin et al., 2012; Zegeye et al., 2013; Zhu, 2013; Osorio and Nanduri, 2015; Tang et al., 2015; Yu and Shi, 2015), can serve as an evaluation tool for quantifying the environmental impacts of various traffic management and traffic control strategies. For example, Panis et al. (2006) developed an integrated model, which is described as the network-wide traffic microsimulation model DRACULA coupled with an instantaneous emission model. In this integrated model, new second-by-second emission functions depending on vehicle speed and acceleration are developed based on actual measurements with several instrumented vehicles driving in real urban traffic situations. Misra et al. (2013) adopted an integrated modeling approach by combining the traffic microsimulation model PARAMICS and the CMEM emission model. Jie et al. (2013) used the microscopic simulation model VISSIM coupled with the VERSIT + emission model. The aforementioned methodology is high-resolution, but has an important drawback that a large number of input variables, e.g., driver behavior attributes (vehicle speed and acceleration), vehicle characteristics (weight or mass) and road geometry (grade), may be required (Osorio and Nanduri, 2015). In contrast, less input data is required for the macroscopic DTA models integrated with the microscopic emission models and this integrated approach can also get a balanced trade-off between computational complexity and accuracy (Zegeye et al., 2013). Yin et al. (2012) presented a network-based macroscopic model coupled with the VT-micro model to investigate the relationships among housing allocation, traffic volume, and CO_2 emissions, but this network-based macroscopic model did not consider time-dependent origin–destination (OD) travel demand. In order to estimate network-wide vehicular emissions, Zegeye et al. (2013) proposed a VT-macro model based on a combination of the macroscopic traffic flow model METANET (which is described as nonlinear difference equations for link traffic flow) and the VT-micro emission model. Here, this macroscopic traffic flow model METANET requires detailed data for all road links and intersections included in the road network for the model setup process, and is thus suitable only for road networks with a simple structure.

In order to estimate traffic-related emissions in urban areas, the macroscopic modeling approach is particularly useful for highly populated urban cities with high population and road densities (Yin et al., 2012). In this study, we integrate a macroscopic DTA model for urban traffic flow with an instantaneous emission model to investigate air pollutants and greenhouse gases emitted by various types of vehicles in a dense urban area of arbitrary shape. These two different models are integrated in such a way that the emission model can get speed and acceleration inputs of the traffic flow from the macroscopic DTA model at every simulation time step. The macroscopic DTA model is described as a 2D hyperbolic system of nonlinear conservation laws with source terms under the hypothesis that all vehicles with the same characteristics, e.g. weight, engine type and size, move like a continuous anisotropic medium. The desired direction of motion for drivers is to minimize the

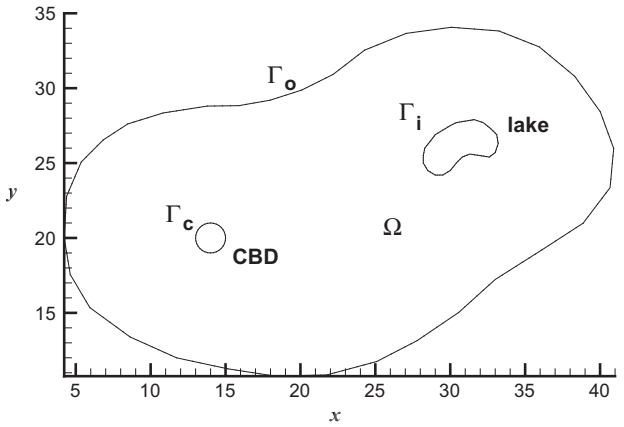

Fig. 1. An urban region of arbitrary shape.

total instantaneous travel cost from origin to destination based on instantaneous traffic information obtained from a radio broadcasting service or route guidance system. The emission model proposed by Panis et al. (2006) is based on empirical measurements which relate vehicle emission to the type, the instantaneous speed and acceleration of the vehicle. A numerical method used to solve the macroscopic DTA model is designed as a Runge–Kutta Discontinuous Galerkin (RKDG) method coupled with a fast sweeping method (FSM) on unstructured meshes (Xia et al., 2008). The proposed model and algorithm are applied to investigate some macroscopic characteristics of urban traffic flow, e.g., the spatial distributions of the flow density and speed, and to predict traffic-related emissions in urban areas of arbitrary shape.

The paper is organized as follows. Section 'Model description' formulates the macroscopic DTA model and the instantaneous emission model. The solution algorithm for the DTA model is described in Section 'Solution algorithms'. Section 'Nu merical results' presents a case study to demonstrate the proposed approach. Finally Section 'Conclusions' provides the conclusions.

Model description

Consider an urban region of arbitrary shape with a single compact central business district (CBD) (Fig. 1). In the region, the road network is dense enough to be viewed as a 2D continuum. The urban region is denoted by Ω (in km^2). Let Γ_o (in km) be the outer boundary of Ω, Γ_c (in km) be the boundary of the compact CBD which represents the travel destination, and Γ_i (in km) be the boundary of an obstruction, such as a lake, where traffic is not allowed to enter or leave.

There are two main components in this methodology: the macroscopic DTA model used to capture traffic flow dynamics and the instantaneous emission model used to calculate exhaust emissions, which are described respectively in Sections 'Macroscopic DTA model' and 'Microscopic emission model'.

Macroscopic DTA model

The macroscopic DTA model is a 2D partial differential equations based on simple laws of fluid dynamics, which describes the behavior of vehicles in the urban road system. Here, we exploit the analogy between the flow of vehicles and fluid particle flows, for which suitable balance or conservation laws can be written. In its continuous version, the model variables are defined here. The density and average velocity of urban traffic flow at location $\mathbf{x} = (x, y) \in \Omega$ and time t are denoted by $\rho(\mathbf{x}, t)$ (in veh/km^2) and $\mathbf{v}(\mathbf{x}, t) = (u(\mathbf{x}, t), v(\mathbf{x}, t))$ (in km/h) where $u(\mathbf{x}, t)$ and $v(\mathbf{x}, t)$ are the speeds in the x- and y-directions, respectively. The desired direction of motion and speed of traffic flow are expressed as a unit vector $\vec{v}(\mathbf{x}, t) = (v_x(\mathbf{x}, t), v_y(\mathbf{x}, t))$ and $U_e(\mathbf{x}, t)$ (in km/h), respectively. The demand distribution of traffic flow is represented by $q(\mathbf{x}, t)$ (in veh/km^2/h), where $q(\mathbf{x}, t)dxdy$ is the traffic demand from the sub-area at $\mathbf{x} \in \Omega$ and time t to the destination Γ_c. Let $\Phi(\mathbf{x}, t)$ (in \$) denote the total instantaneous travel cost of traffic flow from the origin $\mathbf{x} \in \Omega$ to the destination Γ_c, where $\Phi(\mathbf{x}, t) = 0$.

Second-order continuum model

To generate the required traffic data (i.e. second-by-second speed and acceleration of vehicles) for the microscopic emission model, a second-order macroscopic model of urban traffic flow is formulated. Based on the theory of continuous medium mechanics, the traffic density, velocity, and demand for urban traffic flow should satisfy the following equations of conservation of mass and equilibrium of linear momentum to describe the behavior of traffic.

$$\begin{cases} \frac{\partial \rho}{\partial t} + \nabla \cdot (\rho \mathbf{v}) = q, \\ \frac{\partial \mathbf{v}}{\partial t} + (\mathbf{v} \cdot \nabla)\mathbf{v} = \frac{U_e \vec{v} - \mathbf{v}}{\tau} + \bar{\mathbf{c}} \nabla \cdot \mathbf{v}, \end{cases} \tag{1}$$

where $\nabla = \left(\frac{\partial}{\partial x}, \frac{\partial}{\partial y}\right)$ is the spatial gradient operator, $\tau = 0.09$ h is the relaxation time, and $\bar{\mathbf{c}} = \rho P' \mathbf{1}$, where P is the traffic pressure and $\mathbf{1} = (1, 1)$, is the propagation velocity of small disturbance in urban traffic flow. In Eq. (1), the term $\frac{U_e(\rho)\vec{v} - \mathbf{v}}{\tau}$ denotes relaxation which describes the tendency of traffic flow to relax to an equilibrium velocity $U_e\vec{v}$ in time τ, and the term $\bar{\mathbf{c}}\nabla \cdot \mathbf{v}$ describes drivers' anticipation on spatially changing traffic conditions downstream. It is clear that the model (1) is reduced to the AR-type model for vehicular traffic flow (Aw and Rascle, 2000), if the traffic flow marches in 1D space.

The traffic pressure P, which is the analogous to the pressure in the fluid dynamics equations, is typically formulated as an increasing function of the density

$$P(\rho) = \sigma \frac{\rho}{\rho_{max}}. \tag{2}$$

Here, σ is the anticipation coefficient and ρ_{max} is the maximum density of urban traffic flow. The time-varying traffic demand $q(\mathbf{x}, t)$ is assumed to be sensitive to changes in travel cost $\Phi(\mathbf{x}, t)$ and is represented by

$$q(\mathbf{x}, t) = q(\Phi(\mathbf{x}, t), t), \tag{3}$$

which is a monotonically decreasing function of the total instantaneous travel cost $\Phi(\mathbf{x}, t)$ incurred by travelers (Wong, 1998). The desired speed $U_e(\mathbf{x}, t)$ of traffic flow is defined as the following speed-density relationship (Jiang et al., 2011).

$$U_e(\mathbf{x}, t) = U_f(\mathbf{x}) \exp\left[-\beta\left(\frac{\rho(\mathbf{x}, t)}{\rho_{max}}\right)^2\right], \tag{4}$$

where $U_f(\mathbf{x})$ (in km/h) represents the free-flow speed of the vehicles at location $\mathbf{x}$ and β is a positive scalar that is influenced by the urban road area ratio and the geometrics of the free section.

We derive the conservation laws of (1) as follows.

$$\frac{\partial Q}{\partial t} + \frac{\partial F}{\partial x} + \frac{\partial G}{\partial y} = S, \quad \mathbf{x} \in \Omega,\ t \geqslant 0, \tag{5}$$

where

$$Q = \begin{bmatrix} \rho \\ \rho(u + P) \\ \rho(v + P) \end{bmatrix} = \begin{bmatrix} q_1 \\ q_2 \\ q_3 \end{bmatrix}, \quad S = \begin{bmatrix} q \\ \rho \frac{U_e v_x - u}{\tau} \\ \rho \frac{U_e v_y - v}{\tau} \end{bmatrix},$$
$$F = \begin{bmatrix} \rho u \\ \rho u(u + P) \\ \rho u(v + P) \end{bmatrix}, \quad G = \begin{bmatrix} \rho v \\ \rho v(u + P) \\ \rho v(v + P) \end{bmatrix}.$$

The composite Jacobian matrix of the system (5) is defined as $F_n = \frac{\partial F}{\partial Q} n_x + \frac{\partial G}{\partial Q} n_y$, where (n_x, n_y) is a non-zero unit vector. By solving the eigenvalue equation with respect to $\lambda : |F_n - \lambda I| = 0$, we obtain the eigenvalues of F_n as

$$\bar{\lambda}_1 = u n_x + v n_y - \rho P'(n_x + n_y), \quad \bar{\lambda}_2 = \bar{\lambda}_3 = u n_x + v n_y. \tag{6}$$

From (6), the system (5) is strictly hyperbolic, except for $\rho = 0$. Since the traffic pressure P is an increasing function, the system (5) describes the anisotropic behavior of vehicles, which means vehicles respond only to frontal stimuli in the direction of movement.

Determination of desired travel direction

We assume that energy and environmental impacts are not utilized in travelers' decision-making process. Travelers at location $\mathbf{x} \in \Omega$ and time t always tend to select the routes that minimize their total instantaneous travel cost to the destination, based on instantaneous traffic information that is available at the time of decision-making. We define $C(\mathbf{x}, t)$ (in \$/km) as the local generalized transportation cost per unit distance of travel incurred by travelers at location $\mathbf{x}$ and time t, which is formulated as

$$C = \kappa\left[\frac{1}{U_e} + \pi\left(\frac{\rho}{\rho_{max}}\right)^2\right], \tag{7}$$

where κ (in \$/h) denotes the value of time and π (in h/km) is a positive constant. In Eq. (7), the term κ/U_e represents the cost associated with the travel time and the term $\kappa\pi(\rho/\rho_{max})^2$ represents other associated costs, such as a preference for avoiding high-density regions.

Similar to Xia et al. (2008), we obtain the reactive dynamic user-equilibrium condition as the equilibrated flow pattern in the urban system:

$$C\vec{v} + \nabla\Phi = 0. \tag{8}$$

From Eq. (8), the total instantaneous travel cost $\Phi(\mathbf{x}, t)$ of urban traffic flow from origin to destination satisfies the following Eikonal-type equation

$$\begin{cases} \|\nabla \Phi\| = C, & \mathbf{x} \in \Omega, \\ \Phi = 0, & \mathbf{x} \in \Gamma_c. \end{cases} \tag{9}$$

Therefore, the desired direction of motion in the model (1) for urban traffic flow is obtained as

$$\vec{v} = -\frac{\nabla \Phi}{\|\nabla \Phi\|}, \tag{10}$$

which means that travelers in the transportation system always tend to travel along the routes with the lowest total instantaneous travel cost to the destination.

Microscopic emission model

To identify the air quality and to reduce the hazardous emissions affecting the environment and human health, much research has been done in developing the modeling methods of transportation emissions to estimate the emission factors. In this subsection we combine the macroscopic DTA model described in Section 'Macroscopic DTA model' with the instantaneous emission model. This microscopic emission model is established based on empirical measurements relating vehicle emission to the type, the instantaneous speed and acceleration of the vehicle (Panis et al., 2006). We consider several types of vehicles, e.g. petrol cars, diesel cars and LPG cars, and main traffic-related emissions, such as CO_2, NO_x, VOC and PM, based on their potential health impacts and external costs. For other traffic-induced emissions, the potential health impacts are much smaller or their contribution to the total burden of exposure to pollutants is expected to be minimal (Panis et al., 2006). For example, carbon monoxide (CO), known as a very toxic gas, hardly causes any negative effects at low levels in the open air.

Let $U := U(\mathbf{x}, t)$ (in m/s) and $a := a(\mathbf{x}, t)$ (in m/s^2) be the instantaneous speed and acceleration of urban traffic flow in the direction of its motion at $\mathbf{x} \in \Omega$ and time t, respectively. The two instantaneous traffic variables are described as

$$U = \|\mathbf{v}\|/3.6 = \sqrt{u^2 + v^2}/3.6, \tag{11}$$

and

$$a = \mathbf{a} \cdot \frac{\mathbf{v}}{U} \times 10^{-3}/3.6^2. \tag{12}$$

Here, $\mathbf{a} = \left(\frac{du}{dt}, \frac{dv}{dt}\right)$ (in km/h^2) is the acceleration vector of urban traffic flow and is calculated as

$$\mathbf{a} = \frac{U_e(\rho)\vec{\mathbf{v}} - \mathbf{v}}{\tau} + \bar{\mathbf{c}} \nabla \cdot \mathbf{v}, \tag{13}$$

based on Eq. (1) and with $\frac{du}{dt} = \frac{\partial u}{\partial t} + \mathbf{v} \cdot \nabla u$, $\frac{dv}{dt} = \frac{\partial v}{\partial t} + \mathbf{v} \cdot \nabla v$. Mathematically, the instantaneous emission function $E_n^m(x, y, t)$ (in g/s/veh) for each vehicle type and emission type is obtained as (Panis et al., 2006)

$$E_n^m = \max[0.0, (f_1)_n^m + (f_2)_n^m U + (f_3)_n^m U^2 + (f_4)_n^m a + (f_5)_n^m a^2 + (f_6)_n^m Ua]. \tag{14}$$

Here, $n \in \{\text{Petrol car}, \text{Diesel car}, \text{LPG car}\}$, $m \in \{CO_2, NO_x, \text{VOC}, \text{PM}\}$ represent the vehicle type and the emission type, respectively, and $(f_1)_n^m$ to $(f_6)_n^m$ are emission constants determined by non-linear multiple regression techniques. Note that the average speed and acceleration of vehicles have different effects on the four exhaust emissions, which are reflected by the six emission constants, $(f_1)_n^m$ to $(f_6)_n^m$, in the microscopic emission model (14).

Based on the definition of the emission function E_n^m in Eq. (14), the concentration of the emission for the nth vehicle type and the mth emission type at location $\mathbf{x} \in \Omega$ and time t is denoted as $DE_n^m(\mathbf{x}, t)$ (in kg/km^2/h) and is calculated as

$$DE_n^m(\mathbf{x}, t) = 3.6 \times \rho E_n^m. \tag{15}$$

The total emission rate for the nth vehficle type and the mth emission type in the whole urban transportation system at time t is expressed as $TE_n^m(t)$ (in kg/h) and is obtained as

$$TE_n^m(t) = \iint_{\Omega} DE_n^m dxdy. \tag{16}$$

The corresponding cumulative emission for the nth vehicle type and the mth emission type in the whole urban city at time t is defined as $CE_n^m(t)$ (in kg) and is given by

$$CE_n^m(t) = \int_0^t TE_n^m dt. \tag{17}$$

Solution algorithms

In this section, we describe the spacial discretization of the conservation laws (5) by the RKDG method on unstructured meshes. The computational domain Ω is discretized into N_t non-overlapping triangular cells, i.e., $\Omega = \bigcup_{i=1}^{N_t} T_i$, where T_i is the triangular element with an area A_i. We still consider the approximate numerical solution of Eq. (5) as Q and its components belong to the space of piecewise linear functions

$$V_h^1 := \{v \in V | v_{T_i} \in P^1, i = 1, \ldots, N_t\},$$

where P^1 is the space of linear polynomials and which allow discontinuities at inter-element boundaries.

Runge–Kutta Discontinuous Galerkin method

With an arbitrary smooth test function $w(\mathbf{x})$ from the test space V_h^1, the weak form of finite element formulation for any element T_i is given by

$$\frac{d}{dt}\int_{T_i} Qwdxdy + \sum_{j=1}^{3}\int_{E_{ij}} (F,G)\cdot \mathbf{n}_{ij} w dxdy = \int_{T_i} [(F,G)\cdot \nabla w + Sw]dxdy, \tag{18}$$

where $\mathbf{n}_{ij}$ is the unit outward normal vector on each element boundary E_{ij} with length of $|E_{ij}|$.

The solution Q is discontinuous on the boundary of element and thus we replace the flux $\bar{f} := (F,G)\cdot \mathbf{n}_{ij}$ in Eq. (18) with the simple global Lax–Friedrichs numerical flux $h_{ij}(Q^+, Q^-)$ as follows.

$$h_{ij}(Q^+, Q^-) = \frac{1}{2}[\bar{f}(Q^+) + \bar{f}(Q^-) - \alpha(Q^+ - Q^-)], \tag{19}$$

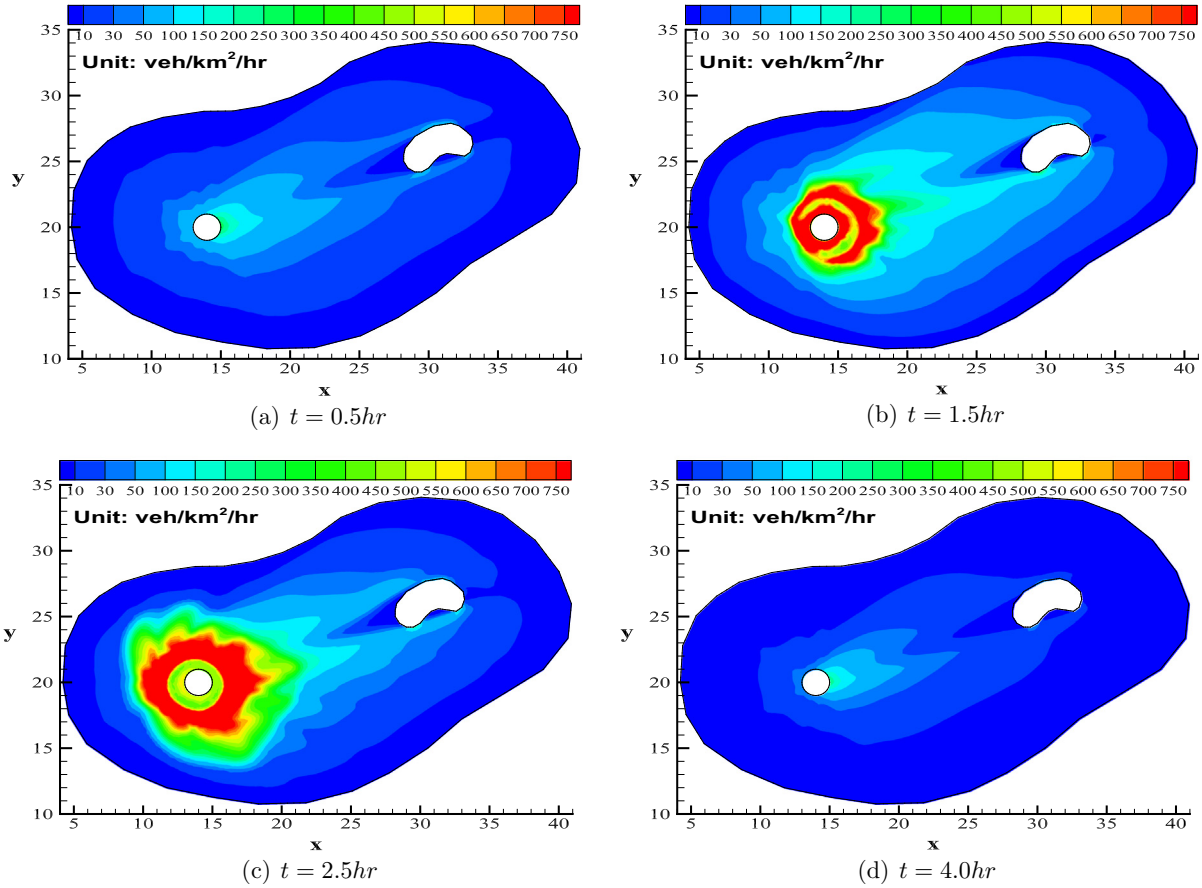

Fig. 2. Spatial distributions of the density of urban traffic flow at different times.

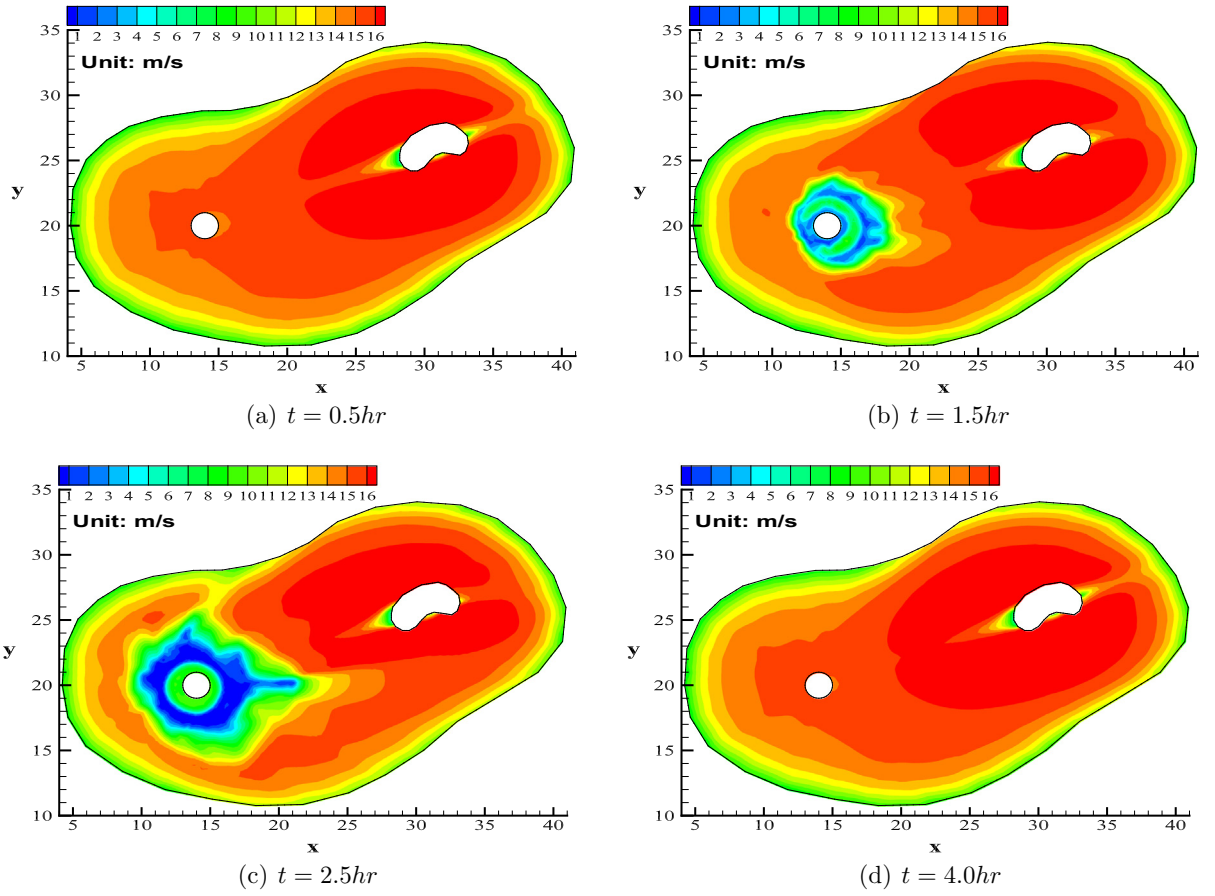

Fig. 3. Spatial distributions of the travel speed of urban traffic flow at different times.

where Q^+, Q^- are the approximations to the values on the edge E_{ij} obtained from the interior and the exterior of T_i, respectively, and α is the viscosity constant taken as $\max_{ij}\{|\lambda_1|, |\lambda_2|, |\lambda_3|\}$. To estimate the integrals in Eq. (18), we apply the following quadrature rules

$$\int_{E_{ij}} (F, G) \cdot \mathbf{n}_{ij} w dx dy \approx \sum_{l=1}^{L} \omega^l h_{ij} (Q^+(\mathbf{x}_{ij}^l, t), Q^-(\mathbf{x}_{ij}^l, t)) w(\mathbf{x}_{ij}^l) |E_{ij}|, \tag{20}$$

$$\int_{T_i} [(F, G) \cdot \nabla w + Sw] dx dy \approx \sum_{k=1}^{K} \omega^k [(F, G) \cdot \nabla w + Sw]|_{\mathbf{x}_i^k} A_i, \tag{21}$$

where are $\mathbf{x}_{ij}^l$ and ω^l are the quadrature points and weights on edge E_{ij}, and $\mathbf{x}_i^k$ and ω^k are those in element T_i.

A second-order TVD Runge–Kutta method is used for the time integration of Eq. (18). To prevent spurious oscillations that tend to be produced around the discontinuities or strong gradients of the approximate solution during computation, we utilize nonlinear limiters described in Cockburn and Shu (1998) to control these oscillations.

Calculation of $\nabla\Phi$ on triangular elements

In Eq. (18), the desired direction of motion $\vec{\boldsymbol{v}}$ in the source term S is unknown. Therefore, we need to first determine $\vec{\boldsymbol{v}}$ by numerically solving the Eikonal-type Eq. (9) at each time step. On each element T_i, the cost potential Φ is assumed to be approximated by the following linear function.

$$\Phi|_{T_i} := \sum_{j=1}^{3} \widehat{N}_j \Phi_j, \tag{22}$$

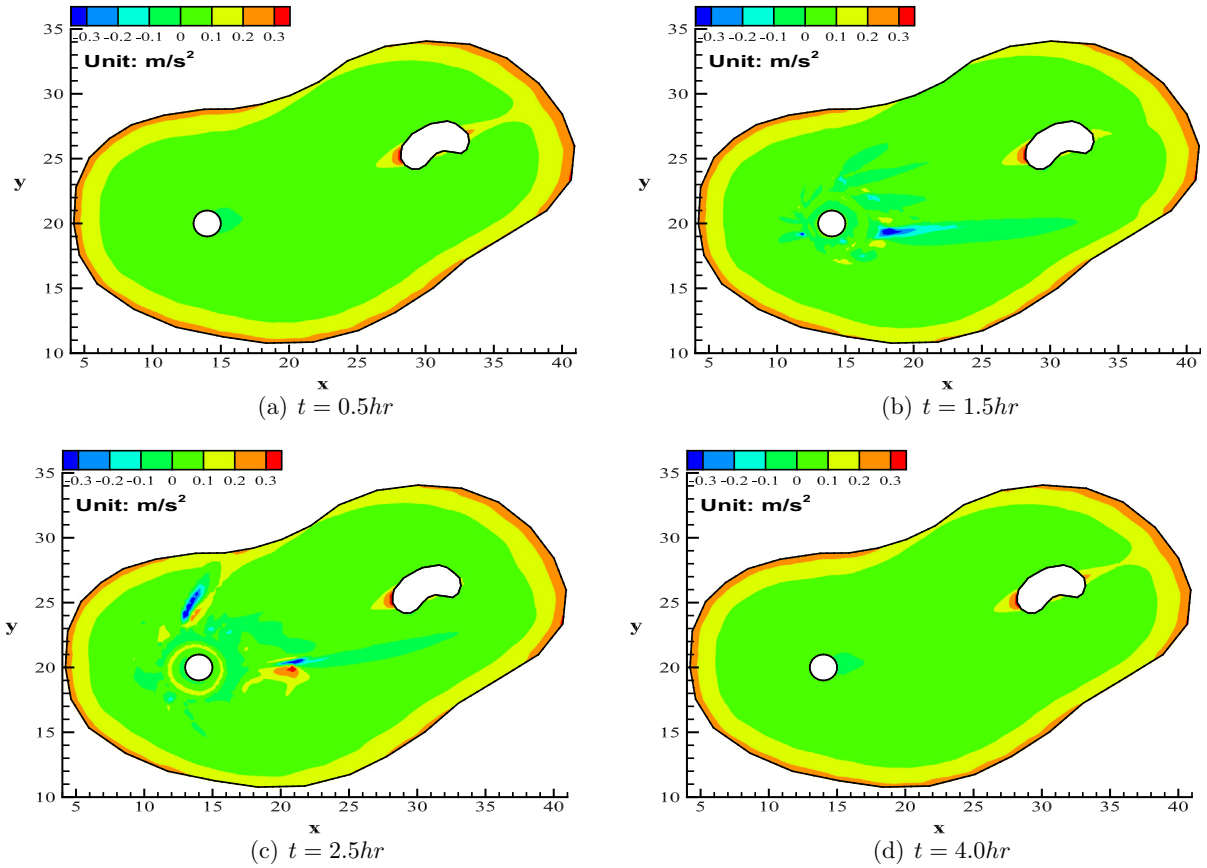

Fig. 4. Spatial distributions of local traffic acceleration of urban traffic flow at different times.

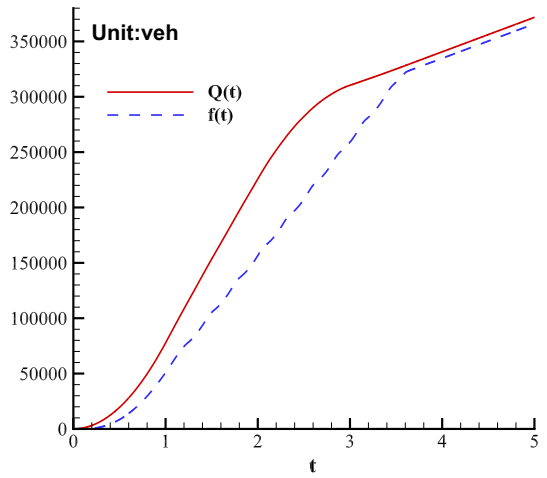

Fig. 5. The plot of the cumulative demand and inflow.

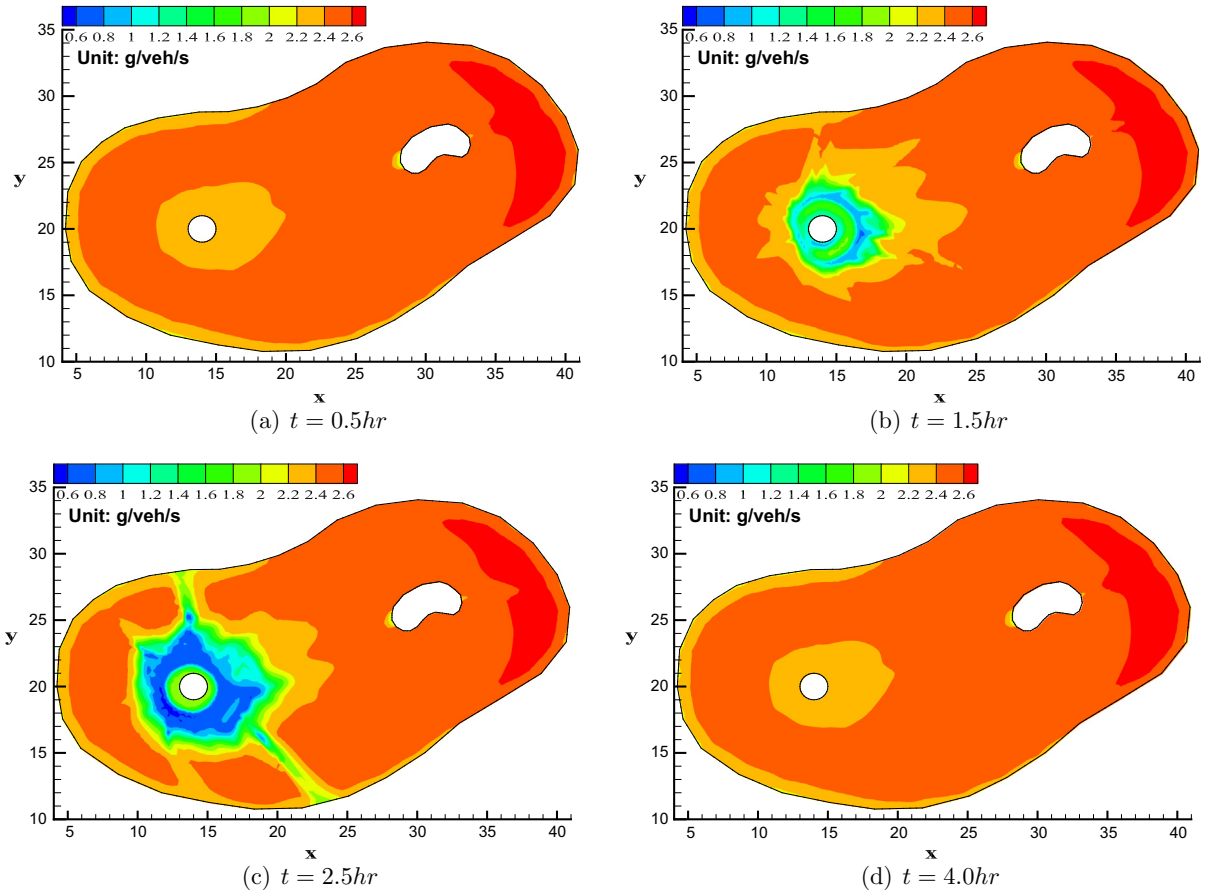

Fig. 6. Spatial distributions of the CO_2 emission rate at different times.

and its gradient is well approximated by the constant vector

$$\nabla \Phi|_{T_i} := \sum_{j=1}^{3} \nabla \hat{N}_j \Phi_j. \tag{23}$$

Here, $\{\widehat{N}_j\}_{j=1}^{3}$ are the Lagrangian interpolation bases and $\{\Phi_j\}_{j=1}^{3}$ are the values of Φ at the vertices of T_i, which are solved through Eq. (9) by the FSM. Further details of this procedure are given in Qian et al. (2007), Xia et al. (2008). The desired direction of motion $\vec{v}$ is computed by Eqs. (10) and (23).

Numerical results

The modeling domain Ω, where a single CBD is located at (14 km,20 km) with a diameter of 1 km, is shown in Fig. 1. The modeling period is 6:00 am–11:00 am, i.e., $t \in$ [0 h,5 h]. Initially, there is no traffic in the urban transportation system, i.e., $\rho(\mathbf{x}, 0) = 0$ veh/km^2 and $\mathbf{v}(\mathbf{x}, 0) = 0$ km/h, $\mathbf{x} \in \Omega$. At the solid walls $\Gamma_o \bigcup \Gamma_i$, the free-slip and non-permeable boundary conditions are applied, i.e., $\partial\rho/\partial\mathbf{n} = 0$ and $\mathbf{v} \cdot \mathbf{n} = 0$. At the outflow boundary Γ_c, $(u, v) \cdot \mathbf{n} = U_f$ and $\partial\rho/\partial\mathbf{n} = 0$. Here, $\mathbf{n}$ is the unit normal vector going out of the region.

The elastic demand function $q(\mathbf{x}, t)$ in Eq. (3) is assumed to be

$$q(\mathbf{x}, t) = q_{max}\left[1 - \gamma_1 \frac{\Phi(\mathbf{x}, t)}{\Phi_{max}(t)}\right] g(t), \tag{24}$$

where $\gamma_1 = 0.35$ is a model parameter specifying the sensitivity of travelers to changes in travel cost, $q_{max} = 320$ veh/km^2/h is the maximum demand of urban traffic flow, and $\Phi_{max}(t)$ is the maximum travel cost in the whole urban area at time t. In Eq. (24), the factor $(1 - \gamma_1 \Phi/\Phi_{max})$ accounts for the greater number of trips that will be generated in the domain with lower

cost, which explains that the traffic demand is elastic. The function $g(t)$ represents the variation factor for demand during the modeling period and is defined by (Jiang et al., 2011)

$$g(t) = \begin{cases} t, & t \in [0\text{ h},1\text{ h}], \\ 1, & t \in [1\text{ h},2\text{ h}], \\ -0.8 \times (t - 3.0) + 0.2, & t \in [2\text{ h},3\text{ h}], \\ 0.2, & t \in [3\text{ h},5\text{ h}]. \end{cases} \tag{25}$$

From the definition of $g(t)$ in Eq. (25), it is a positive continuous function of time during the modeling period. In Eq. (2), $\rho_{max} = 2000$ veh/km^2. In Eq. (4), the parameter β is set to 8 and the free-flow speed function $U_f(\mathbf{x})$ is given by

$$U_f(\mathbf{x}) = U_{max}\left[1 + \gamma_2 \frac{d(\mathbf{x})}{d_{max}}\right], \tag{26}$$

where $U_{max} = 56$ km/h is the maximum speed of urban traffic flow, $d(\mathbf{x})$ is the distance between a location $\mathbf{x} \in \Omega$ and the center of the CBD, d_{max} is the maximum distance from the center of the CBD, and $\gamma_2 = 0.2$. The critical density ρ_c is obtained as $\rho_c = 500$ veh/km^2. In Eq. (7), $\kappa = 60$\$/h and $\pi = 0.01$ h/km. The emission constants in Eq. (14) are specified in Panis et al. (2006) for each vehicle type and emission type.

Fig. 2 shows the density distributions at different times for the evolution of urban traffic flow in four phases. In the first phase ($t = 0.5$ h), traffic flow displays almost a free-flow state within the modeling region and a triangular vacuum region (i.e., an unoccupied area) is formed on the left-hand side of the lake, which describes travelers' optimal route-choice behavior. In the second phase ($t = 1.5$ h), two ring-shaped high-density regions are formed near the CBD, which indicates stop-and-go waves caused by growing traffic congestion occur. Because of the limited capacity of the CBD, more and more travelers gather around the surrounding areas of the CBD and wait in line for entry to the CBD during rush hours. In the third phase ($t = 2.5$ h), traffic congestion still continues but eases somewhat around the surrounding areas of the CBD due to the falling demand. In the fourth phase ($t = 4.0$ h), traffic flow returns to be in a free-flow state. Fig. 3 plots the speed dis-

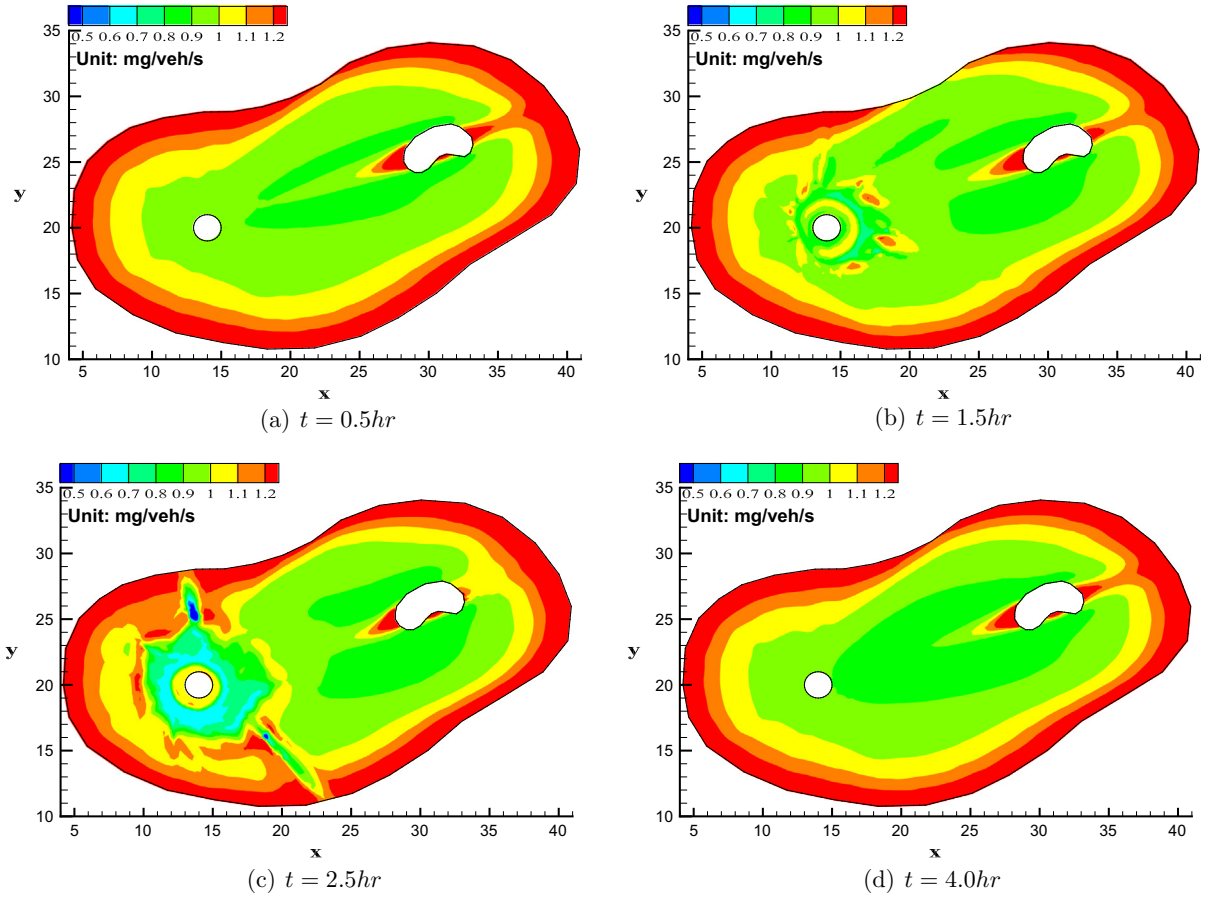

Fig. 7. Spatial distributions of the NO_x emission rate at different times.

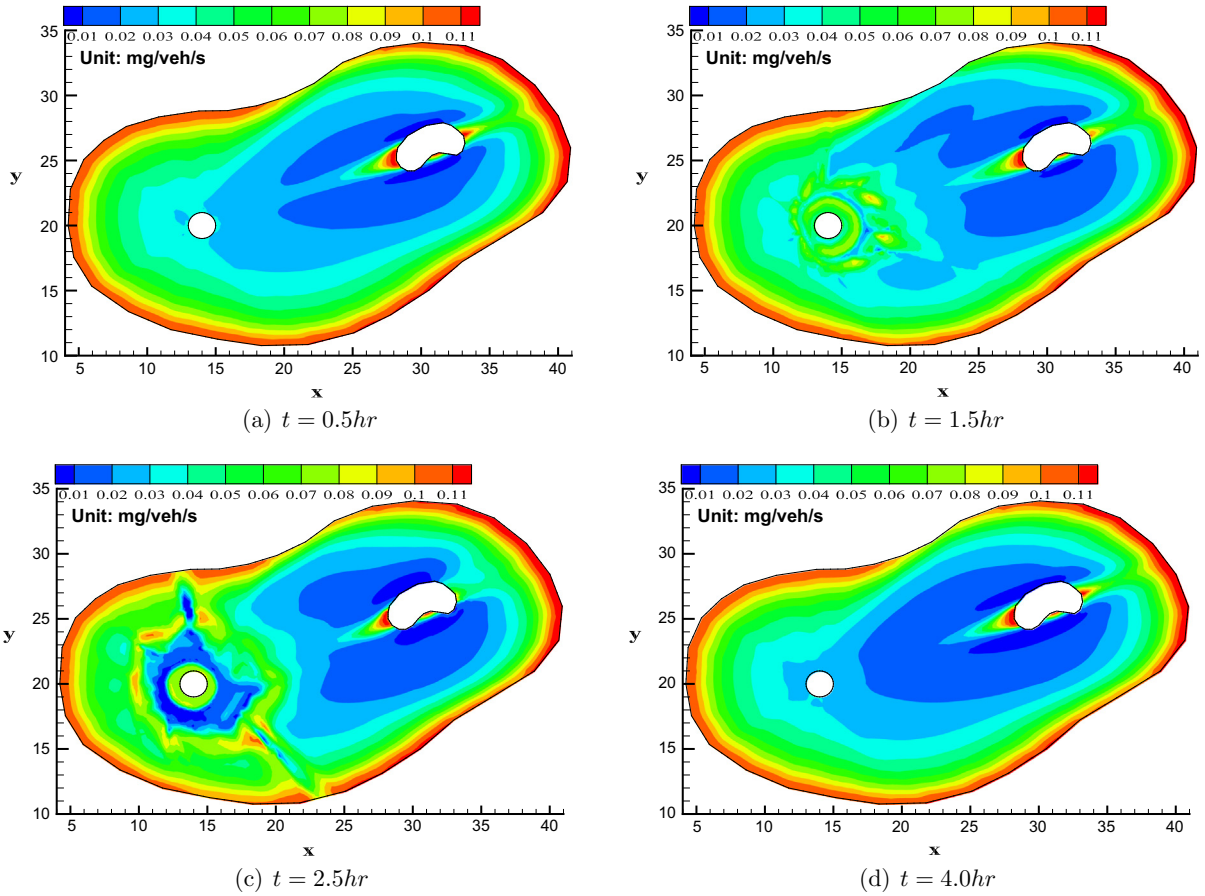

Fig. 8. Spatial distributions of the PM emission rate at different times.

tributions of urban traffic flow at different times. It is observed that the travel speed of vehicles is generally higher in a large areas around the lake where density is lower and is markedly lower near the CBD where density is higher (see Fig. 2(b) and (c)). Fig. 3(b) further illustrates stop-and-go waves occur around the CBD during peak hours. The acceleration distributions of urban traffic flow is depicted in Fig. 4, which shows that the vehicle acceleration is much higher in suburban areas than that near the CBD. This is mainly attributed to low demand and low density in suburban areas. When traffic congestion occurs during peak and off-peak hours, travelers speed up and slow down frequently near the CBD (see Fig. 4(b) and (c)). At other times when the density of urban traffic flow in the whole urban area is relatively low, travelers are accelerating into the CBD. The cumulative demand $Q(t) = \int_0^t \iint_\Omega q dx dy dt$ (in veh) and cumulative inflow $f(t) = \int_0^t \oint_{\Gamma_c} \rho \mathbf{v} \cdot \mathbf{n} ds dt$ (in veh) during the modeling period are shown in Fig. 5. From this figure, we see that there is a large deviation between the $Q(t)$ and $f(t)$ curves from $t = 1.2$ h to 3.6 h, which implies a traffic delay.

Fig. 6 illustrates the spatial distributions of the CO_2 emission rate generated by the petrol cars (i.e., E_1^1) at different times, which are similar to the speed distributions of urban traffic flow shown in Fig. 3. We can observe that the CO_2 emission rate is apparently higher in the regions where the travel speed is much higher, and vice versa. This means the CO_2 emission rate depends mainly on the travel speed of vehicles. The spatial distributions of the NO_x emission rate produced by the petrol cars (i.e., E_1^2) is depicted in Fig. 7. It is clear that the NO_x emission rate in the regions away from the CBD and around the lake is much higher, which is caused by high-speed traffic conditions. In some sub-regions near the CBD, the NO_x emission rate is very high, even though the travel speed is low (see Figs. 3(b) and 7(b)). Fig. 8 plots the spatial distributions of the PM emission rate incurred by the petrol cars (i.e., E_1^4) at different times. The relatively lower PM emission rate appears near the lake where the travel speed is much higher (see Fig. 3), while the PM emission rate is relatively higher in suburban areas where the vehicle acceleration is much higher. This is because main factors that influence transportation emissions are the speed and acceleration of vehicles. From Figs. 6–8, the two emission rates, NO_x and PM, are obviously more sensitive to acceleration behaviors, compared to the CO_2 emission rate. Fig. 9 plots the spatial distributions of the CO_2 concentration emitted by the petrol cars (i.e., DE_1^1) at different times. The CO_2 concentration generally increases with the increase of the density of urban traffic flow. Therefore, the CO_2 concentration is much higher near the CBD where traffic congestion occurs (see Fig. 9(b) and (c)).

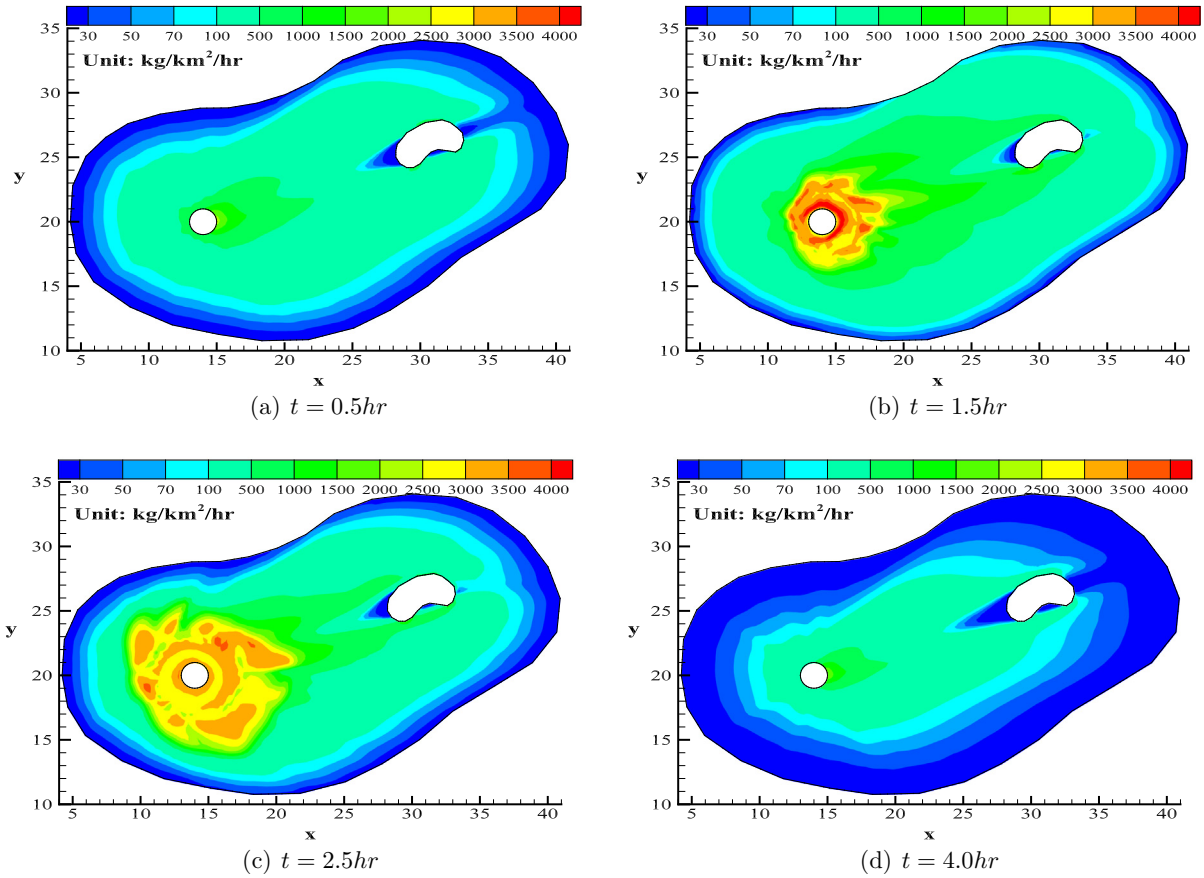

Fig. 9. Spatial distributions of the CO_2 concentration at different times.

To investigate the effects of different types of vehicles on the traffic-related emissions, we compare various exhaust emissions emitted by three types of cars (i.e., the petrol car, diesel car and LPG car). Here, the three types of cars are assumed to have the same instantaneous speed and acceleration calculated by the macroscopic DTA model. Fig. 10 plots the cumulative CO_2, NO_x, VOC and PM emissions (i.e., $CE_n^m, m = 1, 2, 3, 4$) against time t. From Fig. 10(a), the sequence of the cumulative CO_2 emissions emitted by the three types of cars (i.e., $CE_n^1, n = 1, 2, 3$) is $CE_2^1 > CE_1^1 > CE_3^1$ (i.e., the diesel car > the petrol car > the LPG car) before $t = 2.5$ h. As the traffic demand decreases and the travel speed increases after $t = 2.5$ h, the sequence becomes $CE_3^1 > CE_1^1 > CE_2^1$ (i.e., the LPG car > the petrol car > the diesel car), which indicates the emission of CO_2 emitted by the diesel cars is the lowest in the modeling period. However, this type of cars produce the most emissions of NO_x and PM (see Fig. 10(b) and (d)), while other types of cars produce much less NO_x and PM emissions. From Fig. 10(c), the LPG cars generate the most VOC emission, while the diesel cars produce very little VOC emission. In general, each emission type emitted by different types of cars has different characteristics and different sensitivity to changes in a vehicle's speed and acceleration profile. From Fig. 10, it is also observed that the emissions of CO_2 make up the majority of transport emissions. In fact, the cumulative CO_2 emissions for the three types of cars are about 916657.4 kg, 905153.1 kg and 927100.6 kg, which make up about 99.6%, 99.5% and 99.0% of the total cumulative emissions emitted by the three types of cars, respectively.

Fig. 11 shows total emission rates of air pollutants (i.e., NO_x, VOC and PM) in the whole urban area and total cumulative air pollutants at time t for each vehicle type (i.e., $\sum_{m=2}^{4} TE_n^m$ and $\sum_{m=2}^{4} CE_n^m$). From Fig. 11(a), there are apparent fluctuations on the three curves of total emission rates of air pollutants, which are caused by traffic congestion lasting from $t = 1.2$ h to 3.6 h. After $t = 3.6$ h, traffic flow reaches a free-flow state and total emission rates of air pollutants for the three types of cars are constant. The LPG cars produce the most cumulative air pollutants in the modeling period, while the petrol cars generate the least cumulative air pollutants (see Fig. 11(b)). Although the amount of the cumulative CO_2 emission emitted by the diesel cars is lower than that emitted by the petrol cars (see Fig. 10(a)), the diesel cars produce more cumulative air pollutants than the petrol cars do.

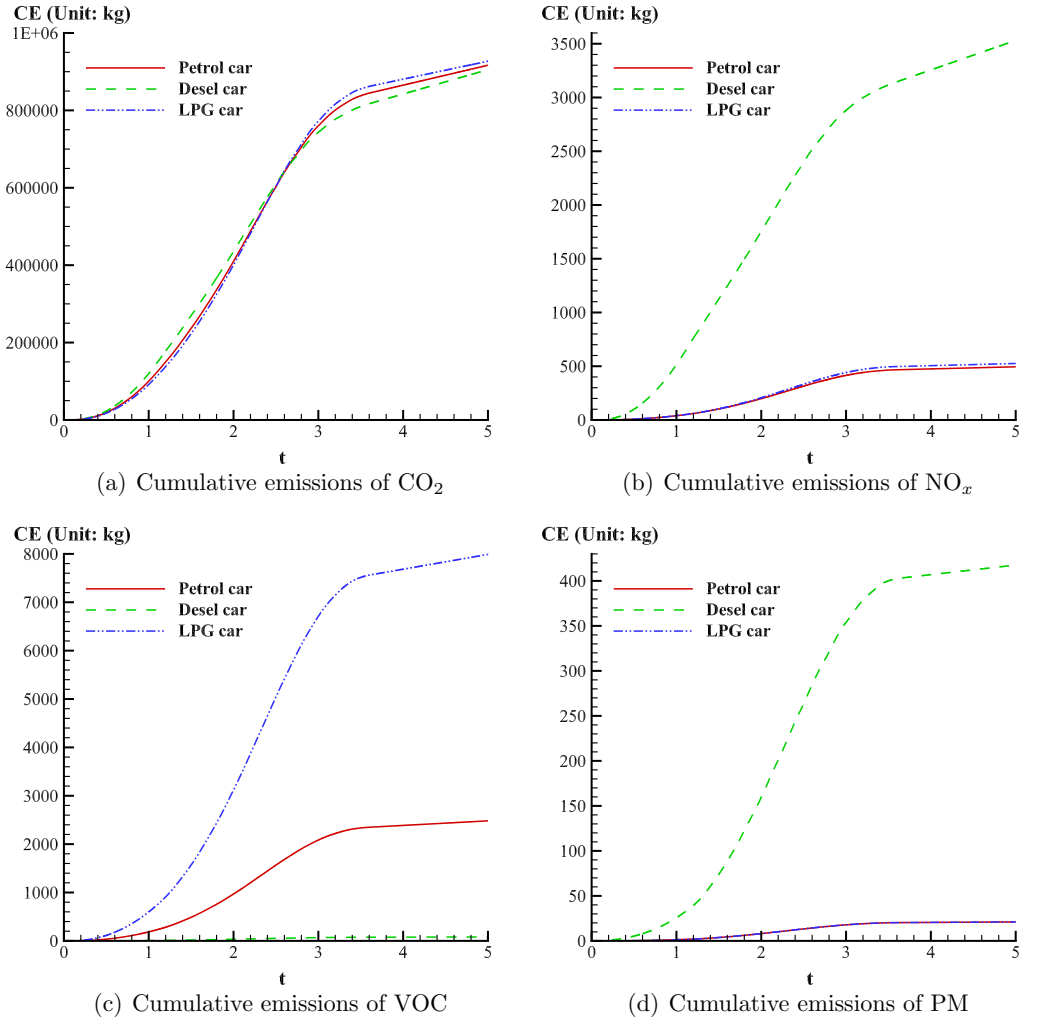

Fig. 10. Comparison of various cumulative emissions of the whole urban city.

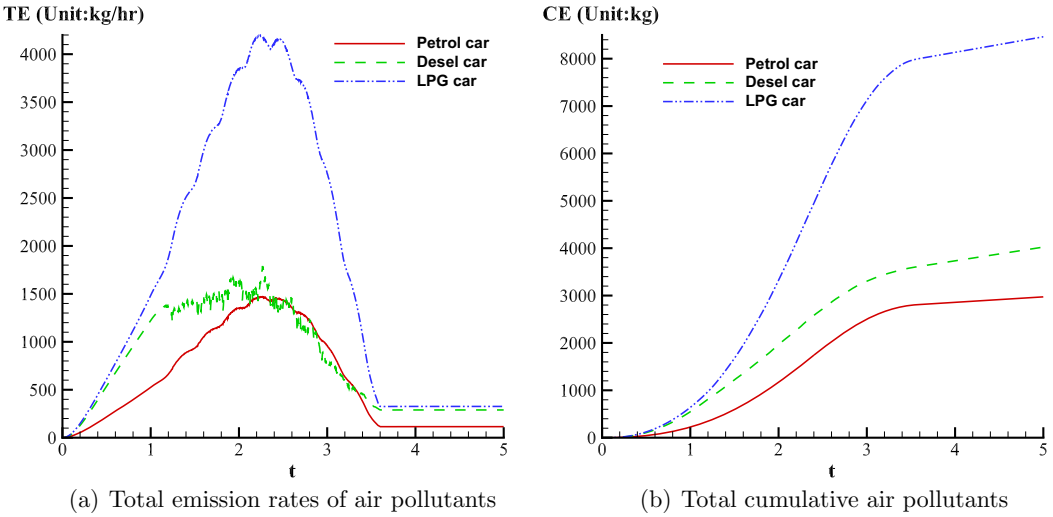

Fig. 11. Total emission rates and cumulative emissions of air pollutants in the whole urban city.

Conclusions

In this paper, we present a general framework used to integrate a macroscopic DTA model with a microscopic emission model to estimate traffic-related emissions in urban areas of arbitrary shape. The macroscopic DTA model can capture the dynamics in the speed and acceleration of vehicles as main input parameters of the emission model. In this model, energy and environmental impacts are not taken into account in travelers' decision-making process and each traveler tends to choose a path with the lowest instantaneous travel cost to the CBD, based on current traffic conditions. The model is solved by the RKDG method for the hyperbolic system coupled with the FSM for the Eikonal-type equation on unstructured meshes. Numerical results verify the applicability of the proposed model and the effectiveness of the solution algorithm from the following two main aspects. On the one hand, this integrated model is able to describe dynamic macroscopic travel/region characteristics (e.g., the density, speed and acceleration distributions of urban traffic flow) and some complex traffic phenomena (e.g., stop-and-go waves), which give a better understanding of user behavior for the control and management of urban road networks. On the other hand, this model is able to estimate various traffic-related exhaust emissions in urban areas (e.g., the spatial distributions of emissions) and therefore can serve as an evaluation tool for quantifying the environmental impacts of various traffic management and traffic control strategies.

Future works will focus on incorporating the effects of multiple vehicle classes and travelers' route-choice decisions on emission levels into the general framework of the macroscopic modeling approach to estimate traffic-related emissions in urban areas.

Acknowledgment

This work was supported by the National Natural Science Foundation of China (Nos. 11202175 and 11372294) and the Research Foundation of Southwest University of Science and Technology (No. 10zx7137).

References

Ahn, K., Rakha, H., Trani, A., Aerde, M.V., 2002. Estimating vehicle fuel consumption and emissions based on instantaneous speed and acceleration levels. J. Transp. Eng. 128, 182–190.
Aw, A., Rascle, M., 2000. Resurrection of "second order" models of traffic flow. SIAM J. Appl. Math. 60, 916–938.
Barth, M., An, F., Younglove, T., Scora, G., Levine, C., Ross, M., Wenzel, T., 2000. Comprehensive modal emissions model (CMEM), Version 2.0, user's guide. University of California, Riverside.
CARB, 2007. EMFAC2007/Version 2.30. User's guide: Calculating emission inventories for vehicles in California. California Air Resources Board, Sacramento, CA, USA.
Cockburn, B., Shu, C.W., 1998. The Runge–Kutta discontinuous Galerkin method for conservation laws V: multidimensional systems. J. Comput. Phys. 141, 199–224.
Cortés, C.E., Vargas, L.S., Corvalán, R.M., 2008. A simulation platform for computing energy consumption and emissions in transportation networks. Transp. Res. Part D 13, 413–427.
Dia, H., Panwai, S., Boongrapue, N., Ton, T., Smith, N., 2006. Comparative evaluation of power-based environmental emissions models. In: Proceedings of the IEEE Intelligent Transportation Systems Conference (ITSC06). Toronto, Canada, pp. 1251–1256.
EPA, 2003. Environmental protection agency (EPA), User's guide to MOBILE, Mobile source emission factor model. EPA402-R-03-010. Ann Arbor, Michigan.
Jiang, Y.Q., Wong, S.C., Ho, H.W., Zhang, P., Liu, R.X., Sumalee, A., 2011. A dynamic traffic assignment model for a continuum transportation system. Transp. Res. Part B 45, 343–363.
Jie, L., Zuylen, H.V., Chen, Y., Viti, F., Wilmink, I., 2013. Calibration of a microscopic simulation model for emission calculation. Transp. Res. Part C 31, 172–184.
Madireddy, M., Coensel, B.D., Can, A., Degraeuwe, B., Beusen, B., Vlieger, I.D., Botteldooren, D., 2011. Assessment of the impact of speed limit reduction and traffic signal coordination on vehicle emissions using an integrated approach. Transp. Res. Part D 16, 504–508.
Misra, A., Roorda, M.J., MacLean, H.L., 2013. An integrated modelling approach to estimate urban traffic emissions. Atmos. Environ. 73, 81–91.
Nejadkoorki, F., Nicholsonb, K., Lakea, I., Daviesa, T., 2008. An approach for modelling CO_2 emissions from road traffic in urban areas. Sci. Total Environ. 406, 269–278.
Niemeier, U., Granier, C., Kornblueh, L., Walters, S., Brasseur, G.P., 2006. Global impact of road traffic on atmospheric chemical composition and on ozone climate forcing. J. Geophys. Res. 111, D09301.
Ntziachristos, L., Samaras, Z., 2000. Copert III computer programme to calculate emissions from road transport: methodology and emission factors (Version 2.1). EEA, Technical Report No. 49. Copenhagen.
Osorio, C., Nanduri, K., 2015. Urban transportation emissions mitigation: coupling high-resolution vehicular emissions and traffic models for traffic signal optimization. Transp. Res. Part B.
Panis, L.I., Broekx, S., Liu, R.H., 2006. Modelling instantaneous traffic emission and the influence of traffic speed limits. Sci. Total Environ. 425, 69–78.
Pataki, D.E., Emmi, P.C., Forster, C.B., Mills, J.I., Pardyjak, E.R., Peterson, T.R., Thompson, J.D., Dudley-Murphy, E., 2009. An integrated approach to improving fossil fuel emissions scenarios with urban ecosystem studies. Ecol. Complex. 6, 1–14.
Peeta, S., Ziliaskopoulos, A.K., 2001. Foundations of dynamic traffic assignment: The past, the present and the future. Netw. Spat. Econ. 1, 233–266.
Qian, J., Zhang, Y.T., Zhao, H.K., 2007. Fast sweeping methods for Eikonal equations on triangular meshes. SIAM J. Numer. Anal. 45, 83–107.
Rossa, F.D., DAngelo, C., Quarteroni, A., 2010. A distributed model of traffic flows on extended regions. Netw. Heterog. Media 5, 525–544.
Saumtally, T., Lebacque, J.P., Haj-Salem, H., 2013. A dynamical two-dimensional traffic model in an anisotropic network. Netw. Heterog. Media 8, 663–684.
Sharma, P., Khare, M., 2001. Modelling of vehicular exhausts – a review. Transp. Res. Part D 6, 179–198.
Smit, R., Ntziachristos, L., Boulter, P., 2010. Validation of road vehicle and traffic emission models – a review and meta-analysis. Atmos. Environ. 44, 2943–2953.
Smit, R., Smokers, R., Rabe, E., 2007. A new modelling approach for road traffic emissions: Versit+. Transp. Res. Part D 12, 414–422.
Szeto, W.Y., Wong, S.C., 2012. Dynamic traffic assignment: model classifications and recent advances in travel choice principles. Cent. Eur. J. Eng. 2, 1–18.
Tang, T.Q., Yu, Q., Yang, S.C., Ding, C., 2015. Impacts of the vehicles fuel consumption and exhaust emissions on the trip cost allowing late arrival under car-following model. Physica A 431, 52–62.
Tao, Y.Z., Jiang, Y.Q., Du, J., Wong, S.C., Zhang, P., Xia, Y.H., Choi, K., 2014. Dynamic system-optimal traffic assignment for a city using the continuum modeling approach. J. Adv. Transport. 48, 782–797.

Vallamsundar, S., Lin, J., 2011. Moves and mobile: a comparison of GHG and criteria pollutant emissions. In: TRB 90th Annual Meeting Compendium of Papers. Washington D.C., USA.
Wong, S.C., 1998. Multi-commodity traffic assignment by continuum approximation of network flow with variable demand. Transp. Res. Part B 32, 567–581.
Xia, L.P., Shao, Y.P., 2005. Modelling of traffic flow and air pollution emission with application to Hong Kong island. Environ. Modell. Softw. 20, 1175–1188.
Xia, Y.H., Wong, S.C., Zhang, M.P., Shu, C.W., Lam, W.H.K., 2008. An efficient discontinuous Galerkin method on triangular meshes for a pedestrian flow model. Int. J. Numer. Meth. Eng. 76, 337–350.
Yin, J., Wong, S.C., Sze, N.N., 2012. Optimization of housing allocation and transport emissions using continuum modeling approach. Asian Transp. Stud. 2, 93–108.
Yu, S.W., Shi, Z.K., 2015. Fuel consumptions and exhaust emissions induced by cooperative adaptive cruise control strategies. Int. J. Mod. Phys. B 29, 1550084.
Zegeye, S.K., Schutter, B.D., Hellendoorn, J., Breunesse, E.A., Hegyi, A., 2013. Integrated macroscopic traffic flow, emission, and fuel consumption model for control purposes. Transp. Res. Part C 31, 158–171.
Zhu, W.X., 2013. Analysis of emission in traffic flow and numerical tests. Phys. A: Stat. Mech. Appl. 392, 4787–4792.